

Black hole algorithm along edge detector and circular hough transform based iris projection with biometric identification systems

Original Scientific Paper

Tara Othman Qadir

Universiti Tun Hussein Onn Malaysia (UTHM)
Faculty of Computer Science and Information Technology
Parit Raja 86400, Johor, Malaysia.
alsaraftara@gmail.com

N.S.A.M Taujuddin

Universiti Tun Hussein Onn Malaysia (UTHM)
Faculty of Electrical and Electronic Engineering
Parit Raja 86400, Johor, Malaysia.
shahidah@uthm.edu.my

Abstract – The circular parameters between the pupil and the iris are found using current iris identification techniques but the accuracy creates an issue for the detection process during image processing. The procedure of extracting the iris region from an eye image using circular parameters can be improved via approximately too many approaches in literature but remain some portions under slightly unconstrained circumstances. In this study, we presented a Black Hole Algorithm (BHA) along the Canny edge detector and circular Hough transform-based optimization technique for circular parameter identification of iris segmentation. The iris boundary is discovered using the suggested segmentation approach and a computational model of the pixel value. The BHA looks for the central radius of the iris and pupil. The system uses MATLAB to test the CASIA-V3 database. The segmented images exhibit 98.71% accuracy. For all future access control applications, the segmentation-based BHA is effective at identifying the iris. The integration of the BHA with the Hough transforms and Canny edge detector is the main method by which the iris segmentation is accomplished. This novel technique improves the accuracy and effectiveness of iris segmentation, with potential uses in image analysis and biometric identification.

Keywords: identification, segmentation, biometric, image-processing, iris detection, accuracy, edge detector, circular hough transformation

1. INTRODUCTION

Iris recognition has quickly emerged as a popular study issue due to its potential use in personal identification considering the rising security demands in our daily lives [1-5]. The iris of the human eye is the annular portion positioned between the white sclera and the black pupil. It has a rich texture created by numerous unique minutes (such as circles, inscriptions, and furrows), among others. Iris is especially helpful for personal identification because it is regarded to be highly discriminative between eyes and stable during a person's lifespan. The human eye is considered a complicated and extremely distinctive biological feature in the field of iris recognition. In this technology, the iris is a tiny, round structure that surrounds the pupil which

is also an essential part of the eye. Each person's iris is unique because of the complex patterns of crypts, furrows, and other distinguishing characteristics that make it unique. Iris patterns are generated during a person's development and are astonishingly stable over the course of a person's lifetime, making them a permanent and trustworthy type of biometric identification. Tucked away inside the iris, the pupil controls how much light enters the eye and adjusts to the surrounding lighting. Iris recognition systems use this interaction between the iris and pupil to offer extremely precise and safe authentication and identification techniques, utilizing the biological wonder of the human eye for cutting-edge technical applications [6, 7]. Fig. 1 depicts the entire human eye, with all of its distinguishing features.

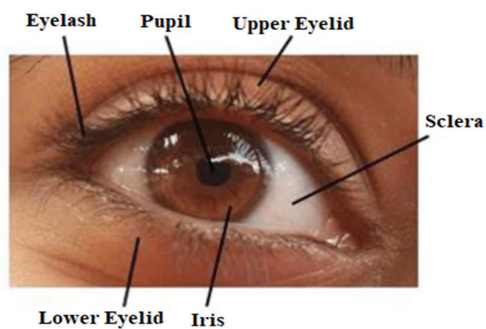


Fig. 1. A generic view of the human eye [6]

For many security applications, rapid development of recognition systems has occurred. This research is driven by the rising market need for automated access control systems with a biometric recognition platform [8]. For human recognition systems, a variety of identification traits have been investigated, including the iris, fingerprint, face, mouth, and ear [9]. The most reliable and consistent recognition biometric, however, is iris-based personal identity systems [10]. In 1993, Daugman [11] wrote about the first successful application of an iris recognition system. A few processes are involved in iris recognition systems, including edge localization, segmentation, normalization, feature extraction, and matching. Accurate segmentation can considerably enhance the performance of the recognition system. The characteristics of the iris' texture vary between any two individuals and between the left and right eyes of the same individual. A sample of the tested database of iris photographs is shown in [12] (Fig. 2). It should be emphasized that the white area is the sclera, and the small black circle represents the pupil of the eye.

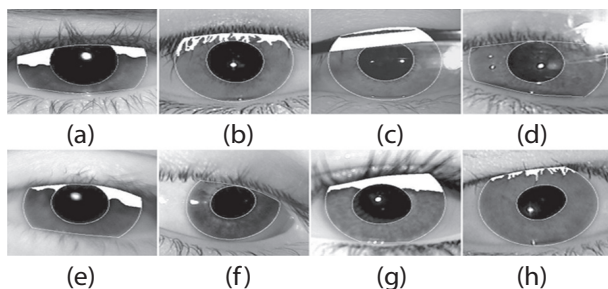


Fig. 2. Examples of iris segmentation by the proposed methods on various challenging iris images. Iris images with (a) severe eyelid occlusion, (b) eyelash occlusion, (c) glass frame occlusion, (d) specular reflections, (e) defocusing, (f) off-axis view angle, (g) motion ghost, and (h) pupil deformation

The iris of the eye is located between the pupil and sclera, though. The key challenge to improving identification accuracy is precisely identifying both the inner and exterior edges of the iris region. It is typical to examine an incomplete iris image, nonetheless. Whereas the area of interest for an iris is obscured by both the eyelid and the eyelash. The outside boundary area cannot be localized using traditional localization tech-

niques. Additionally, the iris's inner area limits, radius, center, and shape are constantly altered by the amount of light falling on the eye pupil.

Due to conflicting boundaries and centers, both the inner and outer circular parameters must be obtained separately [13]. Therefore, a key challenge for biometric iris identification systems is the precise segmentation of incomplete iris boundaries.

High-accuracy iris systems require an accurate segmentation technique. The system's computing complexity may grow, and the time required for iris segmentation may be cut in half. As a result, the iris segmentation problem has been the subject of numerous studies in literature. To determine the iris' boundary, Daugman presented an integro-differential method-based iris identification system [11]. The Hough transform approach was then presented by Wildes to determine the boundaries of the iris [14, 15]. The parameters of the iris boundaries must be searched for using these two traditional methods across the entire parameter space. In [16], the authors used the watershed transform and circle fitting to locate the outer circle, while the inner circle was found using the Canny edge and fitting circle approach [16]. An iris localization approach for imperfect iris data was put forth in [17]. The iris boundaries were located using visible-wavelength light. Edge detection and the identification of the inner and outer circles were performed using the computation of image intensity and the integro-differential operator. To acquire the pupil and iris edges, the researchers also developed an adaptive intensity threshold approach [18]. The boundaries of the inner and outer circles were localized using the circular Hough transformation. Sardar [19] presented hole filling and rough entropy-based iris segmentation. The sclera edge is used to roughly compute the outer circle. However, the next phase of the normalizing process requires more than just utilizing the binarization algorithm. According to [20], the Daugman-rubber sheet normalization requires the parameters of both the inner and outer circles.

The BHA for data clustering was suggested in [21]. The BHA is straightforward to use and has an uncomplicated structure. It features a quick search method for an objective function's ideal parameters. In this research, the BHA is used to determine the iris' inner and outer circular characteristics. This study is divided into the following sections: First, describe some previous studies, and after this, the methodology in which the mechanism of BHA is described. The iris segmentation process is examined through BHA, Canny edge detector, and circular Hough transform. The results and a discussion of the suggested model are covered in the following section. Finally, the conclusion brings this study to a close end.

The BHA's goals for iris border detection and segmentation are useful for vetting accurate and trustworthy iris recognition systems. The purpose is to successfully isolate and extract the iris region from an image.

The end effect of this is to detect and segment the iris boundary with great precision. This guarantees that the extracted iris region closely resembles the iris's true limits.

Here, Section 1 covers the introduction to iris research, and Section 2 presents the research that is pertinent to this matter. The algorithm and its primary parts, as well as the associated methods in the form of methodology, are the foundation of Section 3. Section 4 displays the results of the experiments, and Section 5

concludes this investigation.

2. RELATED WORK

In unregulated situations, iris segmentation approaches can be categorized in a variety of ways. To efficiently investigate the development of the study on this topic, this can be provided three distinct categorizations for these methodologies in this section.

Table 1. Various methods used/developed under some unconstrained factors

Reference	Method	Image scale	Datasets	Limitations
[22]	Adaptive mean shift procedure	Gray-scale	CASIA-V3	Overall performance and reliability of the system
[23]	Robust post-processing Algorithm	Color and Gray-scale	CASIA-V4	Can improve recognition performance with other approaches and improve the unstable bits in the iris code, further investigation is needed for the robust human verification, can search the best possible configuration for feature extraction
[24]	Deep multi-task learning framework, named as IrisParseNet	Color and Gray-scale	CASIA-V1	Can improve the efficiency of the post-processing step or integrate it into the iris segmentation and localization system to form an end-to-end model
[25]	Deep neural network with augmentation method	Gray-scale	CASIA-V1	Advanced augmentation process along with numerical analysis for segmentation
[26]	Dense-Fully Convolutional Network (DFCN), Batch Normalization (BN)	Color and Gray-scale	CASIA-V4	Dense connections are time-consuming, require more training parameters, design for more robust iris segmentation algorithms under non-ideal conditions, and more effective ways of labeling
[27]	Deep-learning classification models	Gray-scale	CASIA-V4	The matching process of computational complexity
[28]	A deep learning framework called SIP-SegNet	Gray-scale	CASIA-V1	This can be expanded upon to create a powerful multi-modal biometric identification system.

Table 1 lists a few well-known techniques for iris segmentation in unrestricted environments along with their limitations. Some methods introduce a novel preprocessing phase for iris segmentation to shorten the search time and lessen the sources of errors. The skin and sclera regions were separated from the iris picture by Sahnoud and Abuhaiba [29] using the K-means algorithm as a preprocessing step. Some other references [23] also used the boundary- and pixel-based approaches.

Among the first suggested and often used techniques that exploit iris boundaries in iris segmentation are Daugman's integro-differential operator [30] and Wildes' method [3]. As a result, research regarding iris region searching is [23] in process. For the reduction of the time searching and minimized the errors are [22]. In [23], the researchers suggested an approach based on a deep multi-task learning architecture named IrisParseNet. To improve the iris identification procedure, it takes advantage of the relationships among the iris, sclera, as well as the pupil.

The researchers developed a deep neural network approach to precisely segment severely damaged iris areas selected from such devices to improve the authentication of the wearable glasses [25]. By combining convolutional neural networks with dense blocks, Chen, Ying, et al. [26] offer an innovative design for segmenting the iris. Their design, DFCN, is where their

name originates. Additionally, several well-known optimization techniques like BN and dropout are used to improve the performance.

Table 2. Comparison accuracy of the iris segmentation with other approaches

Reference	Method	Accuracy (%)
[19]	Rough entropy with circular sector analysis	97.12
[27]	Deep-learning	96.90
[28]	SIP-SegNet	95.11
Proposed algorithm	BHA with Canny edge detector and hough transform	98.71

As can be seen from Table 2, different approaches consistently perform operations with good values across all metrics on different datasets for iris segmentation along with its accuracy comparison. Using a technique dubbed segmentation-less polar representation for iris division, reference [27] combined the noise identification and equalization steps alongside the iris identification stage. This approach can prevent the pupil dilatation issue which may happen under unrestricted contexts because it is built on a deep-learning classification system. In recent research [28], the authors have determined to construct algorithms that concurrently segment more than one visual feature.

The scholars have developed an automated system for iris recognition based on 2D iris images to reduce the dimensionality of iris characteristics without losing pertinent information, feature extraction and feature selection techniques have been applied, including principal component analysis and genetic algorithms. Levenberg-Marquardt's learning rule is used to create the back propagation neural network for iris recognition [31]. Utilizing a voting mechanism, the researchers identify and merge the architectures with the Softmax classifier, concentrating on consensus orientation, using convolutional neural networks with consensus between the architectures. Applying optimization strategies will also prevent overfitting and quicken the learning process [32]. Using geometrical information, the Viola-Jones algorithm divides the human eye into parts and intensifies contrast, all the while designating a circular region that holds the iris. Working on an efficient approach based on the Lagrange interpolating polynomial, it obtains non-circular iris outlines. This system performed better and achieved a higher accuracy rate [33]. The attention mechanism, also known as iris segmentation, is intended to be carried out using an end-to-end encoder-decoder model built on enhanced UNet++. To decrease the number of network parameters and increase training time, efficientNetV2 is chosen as a convolutional block of UNet++. UNet++ incorporates an attention module during the down-sampling phase to reduce irrelevant noise interference and improve the network's capacity to recognize the iris region's discriminability. The technique uses a pruning scheme to generate four distinct performance networks that can be used to recognize iris in a variety of conditions. The method's strong iris segmentation and generalization capability is demonstrated by the experimental findings on iris datasets [34]. An end-to-end, unified deep learning system without normalization to increase iris segmentation and recognition accuracy. Iris segmentation and recognition are handled by a dense spatial attention network (DSANet) and a multi-attention dense connection network (MADNet) in the system. Therefore, several ablation tests are carried out to show how successful MADNet and DSANet are. The best segmentation and recognition performance on low-quality iris images without associated GT data is achieved, according to experiments conducted on three databases in use [35].

3. MATERIALS AND METHODS

The following sections explain the theoretical and experimental aspects of the selected algorithm called BHA which is applied to the iris segmentation along the Canny edge detector and circular Hough transform.

3.1. BLACK HOLE ALGORITHM

The concept of the BHA in space was identified in the last two centuries by Michell and Laplace [36].

Since starlight theoretically cannot pass, it was drawn to the BH. Due to the large mass of matter being com-

pressed into a compact area, a strong gravitational field is detected. According to the phenomenon, anything traveling towards the BH is consumed by the BH before dissipating. The event horizon is a spherical shape that forms the BH boundary. The event horizon's radius is determined by the following equation (1), as shown below [36, 37].

$$R = \frac{2GM}{c^2} \quad (1)$$

Where G , M , and c are the gravitational constant, mass, and the speed of light.

The candidates for the BHA are produced and spread at random throughout the search space [21]. The best candidate with the lowest fitness cost from the previous iteration is the one the candidates turn toward next. Equation (2) shows how the stars are moving in the direction of the black hole. Each star's Euclidean distance from the BHA is computed. Any star that is in the event horizon of the BHA recovery is removed from the optimization. New stars are generated at random within the BHA region's perimeter in the following iteration. The fitness values of each new candidate are then assessed once more. The least-suited candidate is selected as the new BHA. The event horizon radius in the optimization is referred to as the Schwarzschild radius. Schwarzschild radius is calculated by (1) in real space, while it is calculated by equation (3) in BHA [21]:

$$Xi(t+1) = Xi(t) + rand \times (XBH - Xi(t)), i = 1, 2, \dots, N \quad (2)$$

$$R = \frac{f_{BH}}{\sum_{i=1}^N f_i} \quad (3)$$

Where $Xi(t)$ and $Xi(t+1)$ signify the locations of the i th star at iterations t and $t+1$, respectively. $rand$ also denotes a uniform distribution with a 0–1 range. N stands for the number of stars. In the exploration space, X_{BH} identifies the black hole's location. R stands for the event horizon's radius, f_i for the i_{th} star's fitness value, and f_{BH} for the black hole's fitness value.

3.2. CANNY EDGE DETECTOR

By using edge detection, the search space is reduced while maintaining an image's basic structural integrity. One of the common edge detection methods is the Canny edge detection method which has some steps. To reduce noise, the image is smoothed using a Gaussian filter. By using the Pythagorean theorem, the gradient magnitudes of the image are determined with the help of the following equation (4):

$$G = \sqrt{G_x^2 + G_y^2} \quad (4)$$

where G_x and G_y , respectively, represent the corresponding horizontal as well as vertical gradients. The boundaries are then designated in accordance with the gradients' big magnitudes. Edges can be designated as those pixels that are thought to form a portion of an edge through non-maximum suppression. While examination of the appropriate edges is performed via

a thresholding procedure. Besides this, suppressing all edges that are not related to an effective edge to determine the final edges.

3.3. CIRCULAR HOUGH TRANSFORM

This method is used for the searching process of the circles shapes in images this can be found through the equation (5) as stated below:

$$r^2 = (x - a)^2 + (y - b)^2 \quad (5)$$

Where r is considered as the radius of the circle and two points of the circle are x and y whereas the coordinates of the center are a and b . The geometric formulas used for the points of the circle are as follows in equation (6):

$$x = a + r \cos \theta; \text{ and } y = b + r \sin \theta \quad (6)$$

Each point (x, y) on a circle in the original image with a known radius may identify a round centered at (x, y) in the parametric space while the algorithm runs. If all the circles in the parameter space come together at just one location, this location is the exact center of the initial circle (Fig. 3).

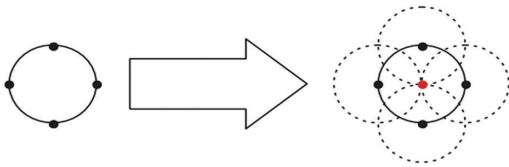


Fig. 3. The principle rule of circular Hough transformation

3.4. IRIS SEGMENTATION

Some sub-level steps are required for this process which is necessary for the iris segmentation.

Step-1: Submission of the paper: Fig. 4 presents the suggested framework of the given conceptual structure. The segmentation model-based BHA optimization is presented using a few procedures along with its activities. As a result, the best fitness value is calculated through the procedure and jumps to the next point which is evaluation.

Step-2: Database: The suggested iris segmentation model is tested using the CASIA-V3 interval database [12]. All the iris photographs were captured using a near-infrared light source and are 8-bit grayscale JPEG files. 2655 photos in all, having a 320 by 280-pixel resolution, were captured from 249 different subjects.

Step-3: Pre-processing: Before testing an image, the following procedures are put into place: The tested image is initially put into the MATLAB workspace. Second, the name of the image that was tested is noted. One of the tested images is called image-1 from the CASIA-V3 database (Fig. 5). The size of the image is examined in the third. The image will become grayscale if it has three layers. The picture matrix is then imported into the MATLAB workspace along with the values of its

pixels. The imparted image matrix is now prepared to determine the iris image border.

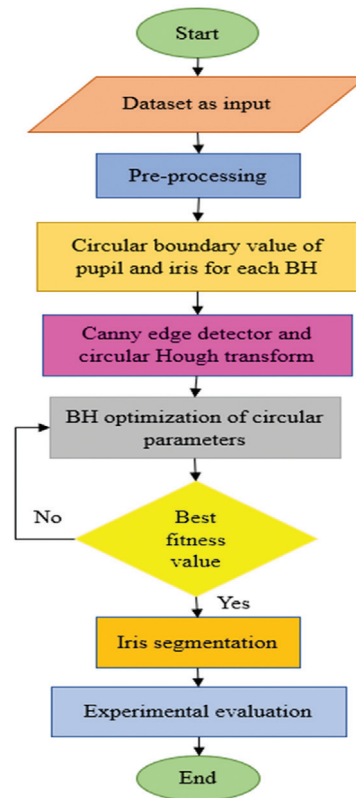


Fig. 4. The framework

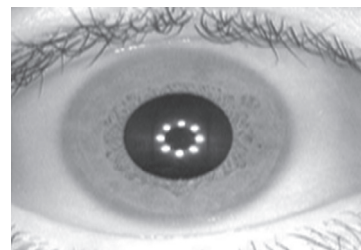


Fig. 5. The input image-1 from the CASIA-V3 for iris segmentation empirical testing

Step-4: Circular boundary detection: The initial problem in this paper is the border identification of the iris image based on pixel values.

As in the vector representations of the iris, which are one-dimensional. In this case, it would seem logical to assume that a boundary pixel should exist between the fifth and sixth pixels.

53 58 55 62 68 123 151 145 141

It would be harder to say that there should be a border in the corresponding region if the intensity difference between the fifth and sixth pixels were larger and the intensity differences between the adjacent neighboring pixels (1st to 4th and 6th to 9th) were smaller. Furthermore, it may be argued that there are numerous edges to this instance. Considered to be a boundary, the fifth pixel can be determined using equation (7).

$$f(x) = \frac{\sum_{i=x+1}^{i=x+n} I(i) - \sum_{i=x-n}^{i=x-1} I(i)}{n} \quad (7)$$

Where $n = 4$ is the fourth-order detection, $I(i)$ is the value of a specific pixel, and $f(x)$ is the boundary value. MATLAB is used to analyze the population of pixels before doing the histogram analysis for the tested image. Fig. 6 shows three populations in three significant regions (pupil, iris, and sclera). Therefore, it is necessary to determine a precise threshold for the size of the intensity difference between two adjacent pixels. Therefore, to determine the boundary of the pupil and iris, two threshold values are required. The multi-level Otsu's technique [38] in MATLAB, which analyses the tested images using the Otsu method, can be used to generate these thresholds. The following results are derived using the multilevel thresholds: the pixel value of the iris region (124 to 165), the pupil (20 to 61), and the sclera area (185 to 219). As a result, considering Equation (7) the pupil boundary's minimal value, $f(x) = 63$ pixels, and the iris's minimum value, $f(x)$, is 20 pixels along a boundary. That establishes the $f(x)$ of BHA. Using limit optimization in MATLAB between 20 and 70. During optimization, any pixel's $f(x) = (20 \text{ to } 70)$ is thought of as a boundary pixel.

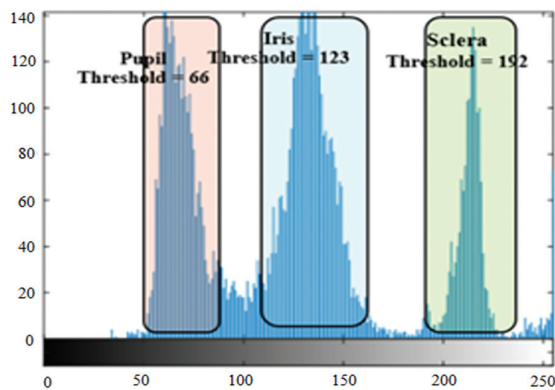


Fig. 6. The numerical values of empirical testing regarding significant regions of the iris

Four times are used to detect border pixels at various angles: 0° and 180° , 45° and 225° , 90° and 270° , and 135° and 315° . That might get worse. The precision of the calculation for various boundary directions (Fig. 7).

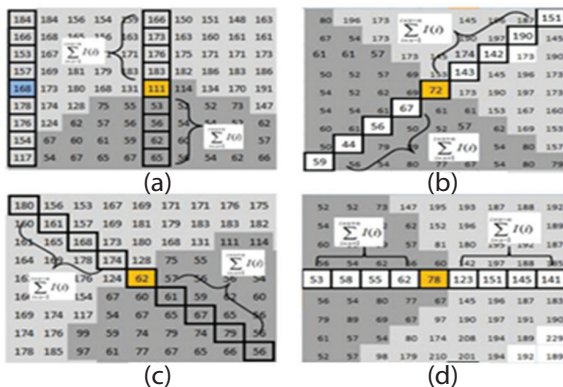


Fig. 7. Recognition of boundary pixels with the help of different angles

Step-5: The BH optimization for pupil boundary:

This work uses the BHA search technique to segment the iris. The BHA can quickly and with fewer computations arrive at the ideal parameters. First, the optimization problem's objective function is set to the circle equation (8). The program looks for the pupil circle's three primary parameters, R_p , X_p , and Y_p , where R_p is the pupil circle's radius in pixels. Additionally, X_p and Y_p show where the circle's center is. Second, the data are analyzed, and the fitness function is determined using the border pixel value equation (7). Thirdly, the BHA generates 100 stars (100 circles) at random for each iteration. Each candidate receives random values for R_p , X_p , and Y_p (Fig. 8). During optimization, the image's size is considered to ensure that all 100 circles are contained within the image.

$$x = r \cos(\theta) + cx; \text{ and } y = r \sin(\theta) + cy \quad (8)$$

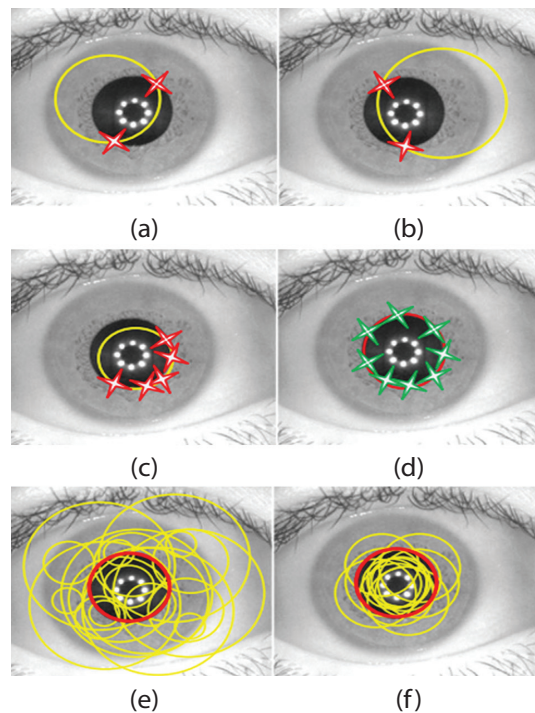


Fig. 8. The BHA operation, (a) star number 7, (b) star number 31, (c) star number 57, (d) star number 73 which is the BH of the first iteration, (e) first iteration the BHA generates randomly 100 stars (100 circles), and (f) second iteration generates 100 circles close to the pupil

To demonstrate (8), the star parameters use a 360-degree step-size circle. Fourth, a black mask zeros image (Istar) with the same dimensions as the input image (320×280) is used to plot this circle. In the original image, an identical circle is formed, but it doesn't touch the image borders. The equation is used to calculate the pixels at the circle's edge (7). When the pixel is located at the border between the iris and the sclera or between the iris and the pupil, the equation (7)'s maximum value might be reached. Fifth, the pixel's computed value that is higher than the thresholds is tallied and recoded using equation (7). For various

angles surrounding this pixel, this calculation is used. The same procedure is applied to the additional pixels that are situated at the circle's edge. For this star, the total number of recorded pixels (the circular border is true) is calculated. Sixth, this candidate's outcome just displays the recorded pixels. The fitness value of the first star (first circle) for unrecorded pixels is calculated using equation (9).

$$f_{star} = 1 - \frac{P_{recorded}}{P_{star}} \quad (9)$$

Where $r = Rp$, θ is the angle, $cx = Xp$, $cy = Yp$, f_{star} is the fitness value of the star, $P_{recorded}$ is the total number of recorded pixels, and $P_{star} = 360$ is the number of star's pixels. For instance, Fig. 8(a) shows the star number 7 produced by the first BHA iteration. On the tested iris image, the seventh star in Fig. 8(a) is shown as a yellow circle. Only at two points does the pupil's border cross that of the yellow circle. Considering this, equation (9)'s calculation yields the high fitness value $f_{7star} = 1 - (47/360) = 0.87$. Furthermore, as shown in Fig. 8, the computation of star number 31 yields a fitness value of $f_{31star} = 1 - (61/360) = 0.83$ Fig. 8(b). The star number 57's fitness value is calculated as $f_{57star} = 1 - (143/360) = 0.60$. Fig. 8(c). Additionally, the star number 73's computation yields a fitness value of $f_{73star} = 1 - (257/360) = 0.28$. Fig. 8(d). According to the framework proposed in Fig. 4, the created circle of star 73 observes the lowest cost fitness. As a result, during the second iteration, star No. 73 is regarded as the pupil's black hole. A further 100 stars are produced in the second iteration using equation (3) BHA. These new stars, however, have circular characteristics that are comparable to those of star 73 from the initial iteration. According to the Equation, the stars' parameters have horizon radius conditions (3). All the newly suggested circles will be placed near the student boundary as a result. Consequently, in just 2 seconds, the best circle representing the pupil boundary is found.

The fitness values of all the stars as well as the remaining 99 stars are subject to this process. Seventh, the BHA updates the location and the black hole candidate for the following iteration by evaluating the fitness values for all the stars. Eighth, in the following iteration, the star whose fitness value is lower than the existing black hole's fitness becomes the new black hole. The fresh random 100 stars migrate in the following iteration toward the new black hole. The BHA generates 100 more circles with parameters that are very similar to those of the new BH and they have the best fitness from the previous iteration. The eight procedures that were used in the initial iteration are then carried out once more. The second iteration's top fitness star advances to the third iteration's BH position, and so forth. The third iteration updates both the BH's location and the stars' proximity to the ideal iris boundary. Finally, this technique can quickly determine the ideal parameters without calculating all the Rp , Xp , and Yp probabilities. The pupil boundary's recognized circle (Fig. 9).

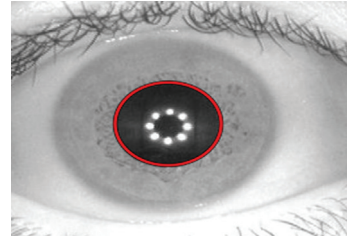


Fig. 9. The boundary of the pupil along its identification

Step-6: The BH optimization for iris boundary: For each star, the BHA can recommend a set of random circle parameters. The top fitness performer from the initial iteration devolves into a black hole for the subsequent iteration. The fitness value of the goal function is gradually increased. The ideal circle that shows the iris border is given once the stop criteria have been met (Fig. 10). The BHA accurately determines the iris boundary's center and radius.

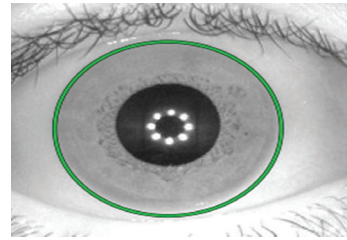


Fig. 10. The boundary of the iris along its identification

Step-7: Iris mask: There are two ways to obtain a logical array mask. First, it is used solely to extract the segmented iris region. Second, it is employed to assess the segmented system's correctness. A 320 x 280 zeros array is created to produce the mask image (I-mask). The iris region is then given one logical value by plotting a filled circle on the I-mask after that. The pupil region is then given 0 logical values by plotting a filled circle on the I-mask. By applying element-wise multiplication, the proposed mask of the segmented iris image (I-mask) is multiplied with the input image (image-1) (Fig. 11), where only the segmented portion of the iris is visible (segmented).

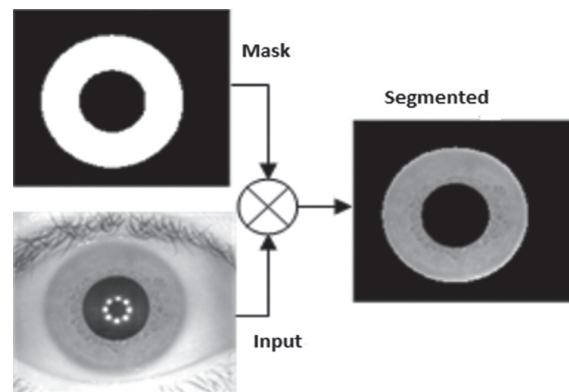


Fig. 11. The process of masking as image-1 and segmenting as results

4. EXPERIMENTAL RESULTS

In this experiment, the accessible iris database is utilized. The chosen segmentation method is tested using the CASIA-V3 database. This database was chosen because it has 2639 images, whereas most of the images in CASIA-V3 had less-than-ideal iris conditions (partial occlusion). Some of the images that were segmented using the BHA are shown in Fig. 12. The outcome shows that the limits of the pupil and the iris are accurately identified. Even though Fig. 12 depicts images with various pupil or iris occlusions and radiuses, the suggested technique is successful in segmenting the iris region.

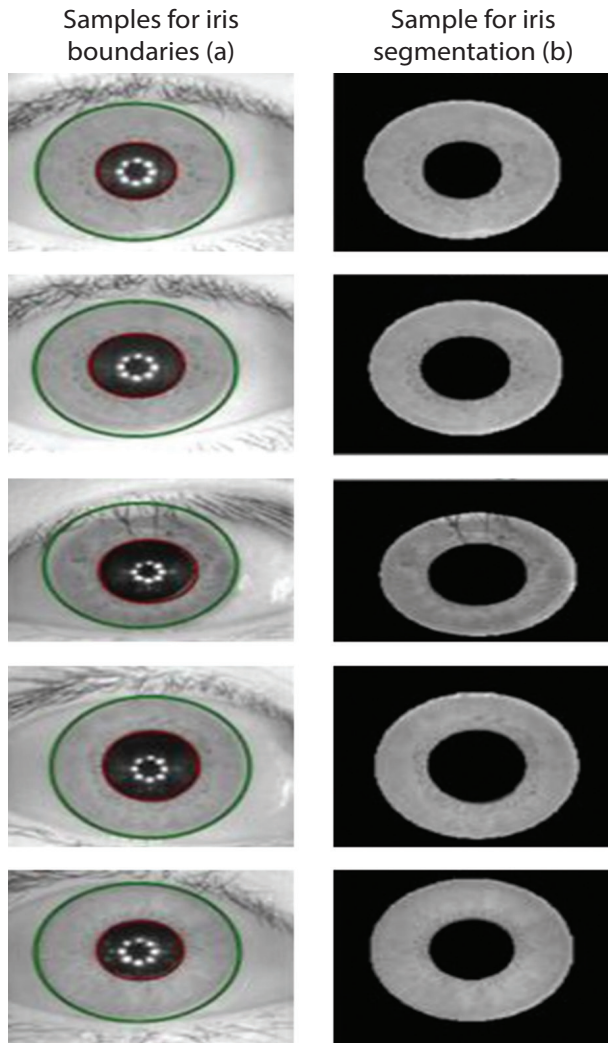


Fig. 12. CASIA-V3 Dataset samples for the detection of the iris edges and segmentation.

Additionally, the suggested algorithm's average accuracy is assessed using the model in [19]. The correctness of each extracted mask (I-mask) is tested using the Images Ground Truth (IGT) of the CASIA-V3 in [39]. The I-mask XOR IGT operation is used to generate mismatched localized pixels (mismatch). Utilizing the I-mask and IGT's confusion matrix function, the performance matrix is computed. According to equation (10), the segmented image's accuracy is expressed as the proportion of correctly predicted pixels, where TN, TP,

FN, and FP stand for true-negative, true-positive, false-negative, and false-positive, respectively. The accuracy of the segmented image-1 using BHA is estimated to be 98.71% (Fig. 13 (a)).

$$Accuracy = \frac{TP+TN}{TP+TN+FN+FP} \quad (10)$$

The average accuracy of all the images is calculated using mismatched images. If image segmentation has a segmented image that, when utilizing (10), has an accuracy lower than 90%. (FN). However, any image segmentation utilizing (10) that achieves an accuracy of more than 90% is correct (TP). The average accuracy of the BHA is tested in this experiment by randomly choosing many images of various subjects. Fig. 13 (b) depicts the confusion matrix of the tested images. The computed average accuracy of all examined images is 8.

$$Average\ accuracy = \frac{(Number\ of\ correct\ segmented\ images)}{(Total\ number\ of\ images)} \times 100\% \quad (11)$$

The average accuracy of the suggested BHA segmentation is 98.71 % according to Equation 11. On average, the suggested BH method has higher segmentation accuracy than [19].

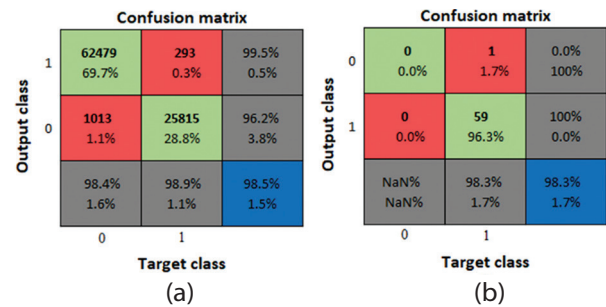


Fig. 13. The confusion matrix along all its parameters percentage

5. CONCLUSION

There are many issues that are frequently formulated as optimization problems, and low-performance optimization techniques suffer from weak or slow convergence to the best solutions for high-performance optimization methods that produce high-quality solutions while consuming the fewest steps. Due to its dependability and practically flawless detection rates, iris recognition has gained popularity. The three primary phases of an iris recognition system are image pre-processing, feature extraction, and template matching. The success of the next feature extraction and template matching stages depends on the iris segmentation stage of the pre-processing procedure. In this study, the CASIA-V3 database has been segmented accurately by using the BHA along the Canny edge detector and circular Hough transform which provides the most appropriate improvement in accuracy. The pupil and iris are segmented using optimization edge boundaries. When optimizing, the complete boundary of the image was deemed satisfactory because of the high segmentation

accuracy of 98.71% obtained by utilizing the combination of the algorithm with the selected methods and the value of pixels. The suggested technique removed the noise from both the eyelid and eyelash consideration in our future study and only split the circular borders. Any iris biometric security system can be made more effective by using the suggested algorithm.

A second way to enhance the algorithm's convergence is to change the randomization parameter so that it gradually drops as the optimum approach. For future work, to improve performance evaluation according to the iris recognition system in non-ideal conditions. It will look for ways to increase accuracy as well as speed so that it can operate in real-time. Future research should focus on expanding this algorithm to color images and evaluating their accuracy for human recognition. Future work should also involve utilizing a minimum of two iris databases to ensure comprehensive experimentation and robust validation of the results.

6. REFERENCES:

- [1] A. K. Jain, A. Ross, S. Prabhaker, "An Introduction to Biometric Recognition", *IEEE Transactions on Circuits and Systems for Video Technology*, Vol. 14, No. 1, 2004, pp. 4-20.
- [2] J. Daugman, "How Iris Recognition Works", *The essential guide to image processing*, Academic Press, 2009, pp. 715-739.
- [3] R. P. Wildes, "Iris Recognition: An Emerging Biometric Technology", *Proceedings of the IEEE*, Vol. 85, No. 9, 1997, pp. 1348-1365.
- [4] K. W. Bowyer, K. Hollingsworth, P. J. Flynn, "Image Understanding for Iris Biometrics: A Survey", *Computer Vision and Image Understanding*, Vol. 110, No. 2, 2008, pp. 281-307.
- [5] C. Tisse, L. Martin, L. Torres, M. Robert, "Person Identification Technique Using Human Iris Recognition", *Proceedings of the Vision Interface*, 27 May 2002, pp. 294-299.
- [6] M. Pathak, N. Srinivasu, V. Bairagi, "Effective segmentation of sclera, iris and pupil in noisy eye images", *Telkomnika (Telecommunication Computing Electronics and Control)*, Vol. 17, No. 5, 2019, pp. 2346-2354.
- [7] H. D. Rafik, S. A. Mahmoudi, A. Reda, M. Boubaker, "A Model of A Biometric Recognition System Based On The Hough Transform Of Libor Masek and 1-D Log-Gabor Filter", *Proceedings of the 5th International Conference on Cloud Computing and Artificial Intelligence: Technologies and Applications*, Marrakesh, Morocco, 24-26 November 2020, pp. 1-9.
- [8] M. Dua, R. Gupta, M. Khari, R. G. Crespo, "Biometric iris recognition using radial basis function neural network", *Soft Computing*, Vol. 23, No. 22, 2019, pp. 11801-11815.
- [9] H. Purohit, P. K. Ajmera, "Optimal feature level fusion for secured human authentication in multimodal biometric system", *Machine Vision and Applications*, Vol. 32, No. 24, 2021, pp. 1-12.
- [10] N. Ahmadi, G. Akbarizadeh, "Hybrid robust iris recognition approach using iris image pre-processing, two-dimensional gabor features and multi-layer perceptron neural network/PSO", *IET Biometrics*, Vol. 7, No. 2, 2018, pp. 153-162.
- [11] J. G. Daugman, "High confidence visual recognition of persons by a test of statistical independence", *IEEE Transactions on Pattern Analysis and Machine Intelligence*, Vol. 15, No. 11, 1993, pp.1148-1161.
- [12] T. Tan, "Note on CASIA-IrisV3", *Chinese Academy of Sciences*, 2011.
- [13] M. Choudhary, V. Tiwari, U. Venkanna, "Enhancing human iris recognition performance in unconstrained environment using ensemble of convolutional and residual deep neural network models", *Soft Computing*, Vol. 24, No. 15, 2020, pp. 11477-11491.
- [14] H. G. Daway, H. H. Kareem, A. R. Hashim, "Pupil detection based on color difference and circular hough transform", *International Journal of Electrical and Computer Engineering*, Vol. 8, No. 5, 2018, pp. 3278-3284.
- [15] B. Zhang, J. Fei, "An Iris Location Algorithm Based on Gray Projection and Hough Transform", *Proceedings of the International Conference in Communications, Signal Processing, and Systems*, Springer, Singapore, 14 August 2019, pp. 1323-1330.
- [16] B. Deshpande, D. Jayaswal, "Fast and Reliable Biometric Verification System Using Iris", *Proceedings of the 2nd International Conference on Inventive Communication and Computational Technologies*, 20 April 2018, pp. 456-460.
- [17] F. Jan, "Non-circular iris contours localization in the visible wavelength eye images", *Computers & Electrical Engineering*, Vol. 62, 2017, pp. 166-177.
- [18] J. A. Ridha, J. H. Saud, "Iris segmentation approach based on adaptive threshold value and circular hough transform", *Proceedings of the International Conference on Computer Science and Software Engineering*, Duhok, Iraq, 16-18 April 2020, pp. 32-37.

- [19] M. Sardar, S. Mitra, B. U. Shankar, "Iris localization using rough entropy and CSA: A soft computing approach", *Applied Soft Computing*, Vol. 67, 2018, pp. 61-69.
- [20] Q. W. Chai, J. W. Zheng, "Rotated black hole: a new heuristic optimization for reducing localization error of WSN in 3D terrain", *Wireless Communications and Mobile Computing*, 2021, pp. 1-13.
- [21] A. Hatamlou, "Black hole: A new heuristic optimization approach for data clustering", *Information Sciences*, Vol. 222, 2013, pp. 175-184.
- [22] R. Chen, X. R. Lin, T. H. Ding, "Iris segmentation for non-cooperative recognition systems", *IET image processing*, Vol. 5, No. 5, 2011, pp. 448-456.
- [23] C. W. Tan, A. Kumar, "Unified framework for automated iris segmentation using distantly acquired face images", *IEEE Transactions on Image Processing*, Vol. 21, No. 9, 2012, pp. 4068-4079.
- [24] C. Wang, Y. Zhu, Y. Liu, R. He, Z. Sun, "Joint iris segmentation and localization using deep multi-task learning framework", arXiv:1901.11195, 2019.
- [25] V. Varkarakis, S. Bazrafkan, P. Corcoran, "A deep learning approach to segmentation of distorted iris regions in head-mounted displays", *Proceedings of the IEEE Games, Entertainment, Media Conference*, Galway, Ireland, 15-17 August 2018, pp. 1-9.
- [26] Y. Chen, W. Wang, Z. Zeng, Y. Wang, "An adaptive CNNs technology for robust iris segmentation", *IEEE Access*, Vol. 7, 2019, pp. 64517-64532.
- [27] H. Proença, J. C. Neves, "Segmentation-less and non-holistic deep-learning frameworks for iris recognition", *Proceedings of the IEEE/CVF Conference on Computer Vision and Pattern Recognition Workshops*, California, 16-20 June 2019.
- [28] B. Hassan, R. Ahmed, T. Hassan, N. Werghe, "Sip-segnet: A deep convolutional encoder-decoder network for joint semantic segmentation and extraction of sclera, iris and pupil based on periocular region suppression", arXiv:2003.00825, 2020.
- [29] S. A. Sahmoud, "Enhancing iris recognition", Islamic University, Department of Computer Engineering, Deanery of Higher Studies, Gaza, Palestine, 2011, Master Thesis.
- [30] J. Daugman, "New methods in iris recognition", *IEEE Transactions on Systems, Man, and Cybernetics, Part B (Cybernetics)*, Vol. 37, No. 5, 2007, pp. 1167-1175.
- [31] M. Garg, A. Arora, S. Gupta, "An efficient human identification through iris recognition system", *Journal of Signal Processing Systems*, Vol. 93, 2021, pp. 701-708.
- [32] D. R. Hammou, S. A. Mahmoudi, R. Adjoudj, "Multi-Biometric Iris Recognition System Using Consensus Between Convolutional Neural Network Architectures", *International Journal of Organizational and Collective Intelligence*, Vol. 12, No. 1, 2022, pp. 1-30.
- [33] F. Jan, S. Alrashed, N. Min-Allah, "Iris segmentation for non-ideal Iris biometric systems", *Multimedia Tools and Applications*, 2021, pp. 1-29.
- [34] G. Huo, D. Lin, M. Yuan, "Iris segmentation method based on improved UNet++", *Multimedia Tools and Applications*, Vol. 81, No. 28, 2022, pp. 41249-41269.
- [35] Y. Chen, H. Gan, H. Chen, Y. Zeng, L. Xu, A. A. Heidari, X. Zhu, Y. Liu, "Accurate iris segmentation and recognition using an end-to-end unified framework based on MADNet and DSANet", *Neurocomputing*, Vol. 517, 2023, pp. 264-278.
- [36] R. Giacconi, "Black hole research past and future", In *Black Holes in Binaries and Galactic Nuclei: Diagnostics, Demography and Formation: Proceedings of the ESO Workshop*, Springer, Garching, Berlin, Germany, 6-8 September 1999, pp. 3-15.
- [37] C. A. Pickover, "Black holes: A traveler's guide", 1st Edition, Wiley-VCH, 1997.
- [38] S. C. Satapathy, N. S. M. Raja, V. Rajinikanth, A. S. Ashour, N. Dey, "Multi-level image thresholding using Otsu and chaotic bat algorithm", *Neural Computing and Applications*, Vol. 29, 2018, pp. 1285-1307.
- [39] H. Hofbauer, F. Alonso-Fernandez, P. Wild, J. Bigun, A. Uhl, "A ground truth for iris segmentation", *Proceedings of the 22nd international conference on pattern recognition*, Stockholm, Sweden, 24-28 August 2014, pp. 527-532.